INSTITUTE OF PHYSICS PUBLISHING JOURNAL OF MICROMECHANICS AND MICROENGINEERING

J. Micromech. Microeng. **13** (2003) 864–872 PII: S0960-1317(03)59395-0

High sensitivity piezoresistive cantilever design and optimization for analyte-receptor binding

Mo Yang, Xuan Zhang, Kambiz Vafai and Cengiz S Ozkan

Mechanical Engineering Department, University of California at Riverside, Riverside, CA 92521, USA

E-mail: cozkan@engr.ucr.edu

Received 10 February 2003, in final form 18 June 2003
Published 14 August 2003
Online at stacks.iop.org/JMM/13/864

Abstract

The mechanical design and optimization of piezoresistive cantilevers for biosensing applications is studied using finite element analysis. The change of relative resistivity of piezoresistive microcantilevers is analyzed in the presence of the chemical reaction at the receptor surface under the condition of oscillating flow. Chemo-mechanical binding forces have been analyzed in order to understand issues of saturation over the cantilever surface. Furthermore, the optimum design using finite element modeling is achieved by modifying the factors pertaining to the geometry of the microcantilevers under the condition of bio-binding. The introduction of stress concentration regions (SCRs) during cantilever fabrication has been discussed, which greatly enhances the detection sensitivity through increased surface stress. Finally, the optimum SCR modified 'C' piezocantilever system for biosensing is designed and the optimal parameters are set for high sensitivity.

(Some figures in this article are in colour only in the electronic version)

1. Introduction

The widespread availability of inexpensive microfabricated cantilevers has resulted in renewed interest in using surface stress-based cantilever sensors as a means of detecting biomolecule absorption. The small size of the microcantilevers and the precise measure of the induced deflection permit the detection of small surface stresses. Changes in the surface properties of the microcantilever through binding or hybridization of analytes to receptor molecules will directly influence its surface stress. This causes the microcantilever to deflect and the deflection is proportional to the analyte concentration. Examples of bindings in biomolecular (receptor/analyte) applications are: antibody-antigen (receptor/analyte) bindings or DNA hybridization of a pair of DNA strands (receptor/analyte) having complementary sequences [1]. The deflection is usually in nanometers and is conventionally measured using optical techniques. Biochips having microcantilevers as sensing elements do not require external power, labeling, external electronics or fluorescent molecules or signal transduction for their operation. These types of biochips can be used in screening certain diseases, such as cancer, and detecting specific chemical and biological warfare agents, such as anthrax and aflatoxin. Alcohol detection in gases has been demonstrated on polymer-coated cantilevers by Jensenius *et al* [2]. The detection of alkanethiol monolayer formation on gold-coated surfaces over cantilevers in gases has been demonstrated by Hansen *et al* [3].

The amount of bending of a cantilever beam can be detected by several read-out systems, including optical detection [4], capacitive detection [5], tunneling detection [6] and interferometric detection. The most commonly used methodology is based on optical detection, where a laser is beam focused on the end of a cantilever, and the position of the reflected beam is measured with a position sensitive photodetector. There are several disadvantages of these techniques. First of all, they require external devices for deflection measurements, in the form of lasers, optical fibers or capacitors. In addition, the alignment and calibration of these external elements are often periodically required. Furthermore, the overall dimensions and power requirements for such detection systems can exceed the requirements of

 © 2003 IOP Publishing Ltd Printed in the UK

field or aircraft deployable devices for biochemical detection purposes. Other difficulties involve the scanning of the whole conjugation area over a cantilever surface; the external detection devices are usually very bulky and do not have the flexibility for that purpose. These disadvantages can be avoided by integrating the detection elements or devices into the cantilever. When a piezoresistive material such as doped silicon is strained, its electrical conductivity is changed. The change in the resistivity can be most conveniently measured by using a Wheatstone bridge. Piezoresistive microcantilevers are ideal for detecting the changes in surface stress due to cantilever deflection upon binding of biochemical agents; they do not require external detection devices, they do not require tedious alignment, and they can be made to fit in an integrated electromechanical system [7].

The fractional change in resistance ($\Delta R/R$) of a piezoresistive cantilever is described by the following expression [8]

$$\frac{\Delta R}{R} = \beta \frac{3\pi_L(1-\upsilon)}{t}(\sigma_1 - \sigma_2) \tag{1}$$

where π_L is the piezoresistive coefficient of silicon along the $\langle 110 \rangle$ axis, σ_1 is the longitudinal stress, σ_2 is the transverse stress, t is thickness of cantilever, υ is Poisson's ratio, and β is a factor that adjusts for the thickness of the piezoresistor [9]. From equation (1), the ratio $(\Delta R/R)$ is proportional to differential stress $(\sigma_1 - \sigma_2)$. Differential stress distribution over a cantilever surface depends on the geometric factors of the layers and the chemo-mechanical forces between the biomolecules and the capture or hybridization layers. Therefore, the deflection signal can be increased by maximizing differential stress $(\sigma_1 - \sigma_2)$ by changing the geometric factors. However, a thorough study is needed to explore the change of relative resistivity of piezoresistive microcantilever in the presence of a chemical reaction at the receptor surface under the condition of the dynamic effect of an oscillating flow representing flow turbulence on the microcantilever. The design principle of different geometries for high sensitivity is also not clear.

In this work, the change of relative resistivity of piezoresistive microcantilever has been analyzed in the presence of a chemical reaction at the receptor surface under the condition of the dynamic effect of an oscillating flow representing flow turbulence on the micocantilever. Furthermore, this analysis will help in establishing the parameters that can be used in finite element modeling for determining the effect of chemo-mechanical binding of an analyte onto the microcantilever surface and also the effect of relative resistivity of the piezoresistive microcantilever due to the previously mentioned conditions. Finally, through this work we establish the optimum parameters involved in enhancing surface stress in piezoresistive microcantilevers. The optimum design using finite element modeling is achieved by modifying the factors pertaining to the geometry of the microcantilevers under the condition of bio-binding. The optimization has been achieved by implementing the analytically determined parameters into the finite element modeling which produces an enhancement of surface stress in the piezoresistive microcantilevers.

2. Analysis

The differential stress $\Delta\sigma$ is proportional to the number of analyte molecules attached to the receptor surface. This relation has the following form according to Lavrik *et al* [10]

$$\Delta\sigma = \Delta G\, \Gamma M^{-1} \tag{2}$$

where ΔG is the change in the Gibbs free energy caused by the adsorption process, Γ is the mass of the bound analyte molecules per unit area and M is the molar mass of the analyte. This equation is based on the Dupre equation that relates the surface free energy of the substrate and the adsorbate and the work of adhesion.

The first-order chemical reaction equation is

$$\frac{\mathrm{d}N_\mathrm{b}}{\mathrm{d}t} = k_\mathrm{ad}(N_0 - N_\mathrm{b}) \tag{3}$$

where k_ad, N_b and N_0 are the adhesion rate, cumulative number of analytes molecules and the total number of analytes molecules bound on the substrate after the experiment, respectively. The adhesion rate according to Chang and Hammer [11] is

$$k_\mathrm{ad} = k_\mathrm{f} C_\infty N_\mathrm{r} \tag{4}$$

where k_f, $C_\infty$and N_r are the effective reaction rate, surface analyte concentration and the number of available receptors, respectively. The results of Swift *et al* [12] agree with the previous equation. Thus, equation (3) reduces to

$$\frac{\mathrm{d}N_\mathrm{b}}{(N_0 - N_\mathrm{b})} = k_\mathrm{f} C_\infty N_\mathrm{r}\, \mathrm{d}t. \tag{5}$$

The analyte concentration due to turbulence can be written according to

$$C_\infty = (C_\infty)_0 - \beta_\mathrm{c} \sin(\omega t) \tag{6}$$

where $(C_\infty)_0$ and β_c are the mean free stream analyte concentration and the amplitude of concentration. k_f increases with the vibration frequency of the molecules [11]. Also, Ramakrishnan and Sadana [13] show that the turbulence at the receptor surface, which is produced by varying the surface roughness of the receptor, results in an increase in the effective reaction rate at the surface. They ascribed it to the mixing effect that the turbulence produces, which results in increasing the vibration frequency of the molecules. Turbulence at the receptor surface can also be produced by disturbances in the flow. In this paper, the relation between the effective reaction rate and the turbulence frequency is taken to be linear for simplicity.

$$k_\mathrm{f} = \bar{k}_\mathrm{f}(1 + a\omega) \tag{7}$$

where $\bar{k}_\mathrm{f}$ and a are the effective reaction rate in the absence of the turbulence and a constant, respectively. Thus, equation (5) reduces to

$$\frac{\mathrm{d}N_\mathrm{b}}{(N_0 - N_\mathrm{b})} = \bar{k}_\mathrm{f}(1 + a\omega)[(C_\infty)_0 - \beta_\mathrm{c} \sin(\omega t)]N_\mathrm{r}\, \mathrm{d}t. \tag{8}$$

This is a first-order differential equation and has the following solution given that $N_\mathrm{b}(t = 0) = 0$:

$$N_\mathrm{b} = N_0\big[1 - \mathrm{e}^{-\bar{k}_\mathrm{f} N_\mathrm{r}(1+a\omega)((C_\infty)_0 t + \frac{\beta_\mathrm{c}}{\omega}(\cos(\omega t) - 1))}\big]. \tag{9}$$

The parameter N_b can be related to Γ by the following relation

$$\frac{N_\mathrm{b}}{A_\mathrm{m}} = \Gamma M^{-1} A \tag{10}$$

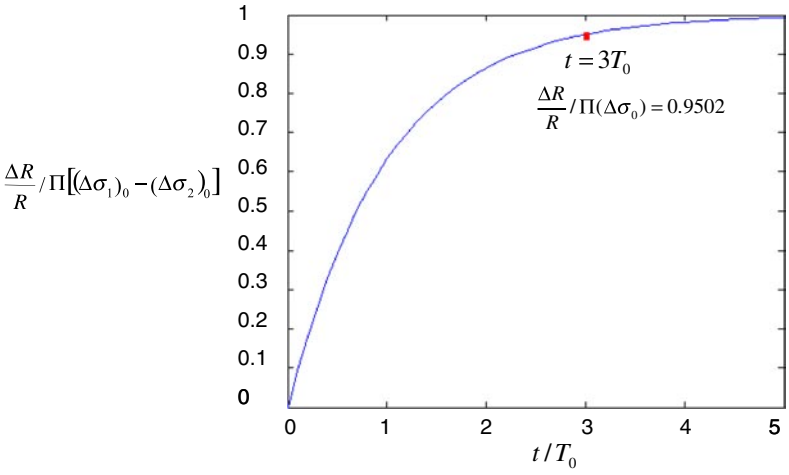

Figure 1. Resistance changes versus time due to analyte-receptor binding.

where Γ, M, A and A_m are the mass of the adsorbate per unit area, molar mass, number of analyte molecules per mole and the area of the receptor coating, respectively. Therefore, the time history for the surface stress can be related to equation (9) by applying equations (2) and (10) and the result is

$$\Delta\sigma = (\Delta\sigma)_0\left[1 - e^{-\bar{k}_f N_r(1+a\omega)((C_\infty)_0 t+\frac{\beta_c}{\omega}(\cos(\omega t)-1))}\right] \quad (11)$$

where $(\Delta\sigma)_0 = \Delta G N_0 A_m^{-1} A^{-1}$. Thus, equation (1) can be reduced to

$$\frac{\Delta R}{R} = \Pi[(\Delta\sigma_1)_0 - (\Delta\sigma_2)_0] \times\left[1 - e^{-\bar{k}_f N_r(1+a\omega)((C_\infty)_0 t+\frac{\beta_c}{\omega}(\cos(\omega t)-1))}\right] \quad (12)$$

where $\Pi = \beta\frac{3\pi_L(1-\upsilon)}{t}$ is the piezoresistor coefficient, $(\Delta\sigma_1)_0 = \Delta G_1 N_0 A_m^{-1} A^{-1}$, $(\Delta\sigma_2)_0 = \Delta G_2 N_0 A_m^{-1} A^{-1}$. It was found that the adhesion rate is inversely proportional to the translational velocity, u, of the analyte molecules for a wide range of translational velocities. According to the data present in the work of Pritchard *et al* [14], the effective binding rate can be linearly correlated to the analyte rolling velocity and the translational velocity, such that

$$\bar{k}_f = \bar{k}_{fo} - b|u| \quad (13)$$

where $\bar{k}_{fo}$ and b are constants greater than zero. Therefore, equation (12) is further reduced to

$$\frac{\Delta R}{R} = \Pi[(\Delta\sigma_1)_0 - (\Delta\sigma_2)_0] \times\left[1 - e^{-(\bar{k}_{fo}-b|u|)N_r(1+a\omega)((C_\infty)_0 t+\frac{\beta_c}{\omega}(\cos(\omega t)-1))}\right]. \quad (14)$$

If we ignore the effect of turbulence, i.e. when the flow is fully developed, equation (14) is simplified to

$$\frac{\Delta R}{R} = \Pi[(\Delta\sigma_1)_0 - (\Delta\sigma_2)_0][1 - e^{-(\bar{k}_{fo}-b|u|)N_r C_\infty t}]. \quad (15)$$

Here we define $T_0 = 1/(\bar{k}_{fo} - b|u|)N_r C_\infty$. When $t \geqslant 3T_0$, the change of relative resistance almost reaches the maximum (figure 1). This is because, when the analyte concentration reaches a saturated level, the process of binding will reach a state of dynamic equilibrium. The analyte concentration is uniformly distributed over the reaction surface.

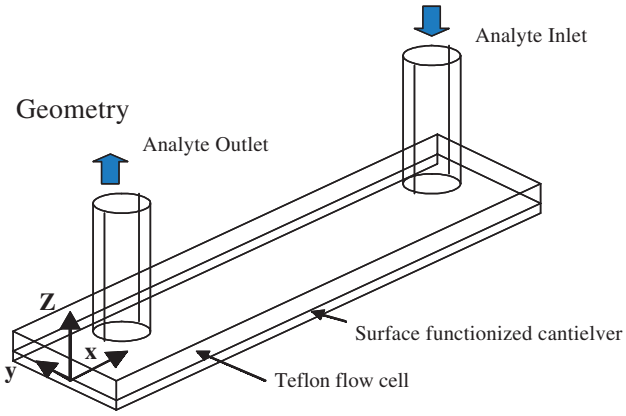

Figure 2. Model of the sensogram.

3. Finite element modeling simulation and design

We have developed a finite element computational model for simulating the chemo-mechanical surface stresses due to analyte binding on functionalized surfaces based on the former analysis with CFDRC™. We have conducted simulations using a model where a substrate functionalized with the binding molecules is inserted in a thin plate-shaped flow cell. The simulation system is schematically illustrated in figure 2. A liquid solution containing the analyte passes through an orifice with a circular inlet port connecting to the flow cell. A functionalized substrate on which the binding molecules are attached is located in the bottom of the flow cell. For the simulations, we have assumed an arbitrary set of analyte and binding molecules that have a strong binding affinity. The initial analyte concentration in the bulk solution was taken to be 5×10^{-6} M, and the inlet volumetric flow rate was 300 μl min^{-1} (table 1).

The cantilever beam in this work is 30 μm wide and 120 μm long with a thickness of 1 μm. The piezoresistive layer has a depth of 0.1 μm. The length of the piezoresistive layer is 80 μm, which covers the most area near the support. The capture area is located at the top surface of the cantilever. Table 2 shows the geometrical parameters used in this paper.

Table 1. List of the partial parameters used in the chemo-mechanical binding analysis.

Property	Value
Association rate constant, K_a	1×10^9 M^{-1} s^{-1}
Dissociation rate constant, K_d	0.001 s^{-1}
Initial analyte concentration in the bulk solution, C_∞	5×10^{-6} M
Maximum possible surface analyte concentration, P_s	2×10^{-6} mole m^{-2}
Density of sample	1000 kg m^{-3}
Viscosity of sample	0.86×10^{-6} m^2 s^{-1}
Diffusivity of analyte, D	4×10^{-7} cm^2 s^{-1}
Inlet volumetric flow rate, Q	300 μl min^{-1}

Table 2. A list of the geometrical parameters used in this paper.

Parameters	Nomenclature
Length of cantilever	L
Width of cantilever	W
Thickness of elliptical holes	th
Transverse axis length of elliptical holes	R_t
Longitudinal axis length of elliptical holes	R_l
Distance between elliptical holes	L_h
Distance between the first hole and the support	L_d
Length of cantilever close to the support for variable width study	L_v
Length of cantilever at the end for variable width study	W_v
Width of cantilever close to the support for variable width study	L_e
Width of cantilever at the end for variable width study	W_e

It can be seen from figure 2 that the model exhibits symmetry about the XZ plane. This symmetry can be utilized for the analysis by building a grid that uses only half of the geometry (the symmetrical half about the XZ plane) and applying the symmetry BC on that plane. The model is also symmetric about its center, about a plane parallel to the YZ plane. This symmetry cannot be used because the flow is not symmetric about this plane (one is an inlet tube and the other is an outlet tube for the fluid flow, hence the asymmetry about that plane.)

3.1. Geometrical analysis of a piezoresistive cantilever beam

In general, the adsorption of molecules to a binding surface causes a change in the surface free energy, which is also called the surface tension. The mechanical response of a biosensing cantilever is caused by a change in the surface stress upon binding and hybridization of biomolecules. The change of relative resistivity is proportional to the stress difference, so the sensitivity of the cantilever can be enhanced by maximizing this stress difference ($\sigma_1 - \sigma_2$). The resonance frequency of microcantilevers is very sensitive to the properties of the microcantilever surface. Changes in the surface properties of the microcantilever through binding or hybridization of analytes to receptor molecules will directly influence its resonance frequency by changing the overall cantilever mass and the thickness of the binding layer. The dynamic effects of flow turbulence in the micofluidic chamber will cause associated noise due to microcantilever deflection, which will decrease the signal-to-noise ratio (SNR). So the parameters

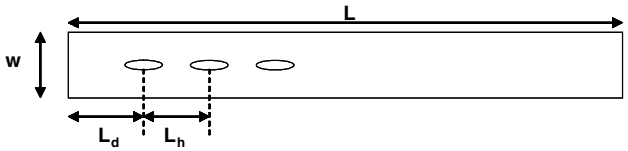

Figure 3. Top view of a piezoresistive microcantilever with elliptical holes.

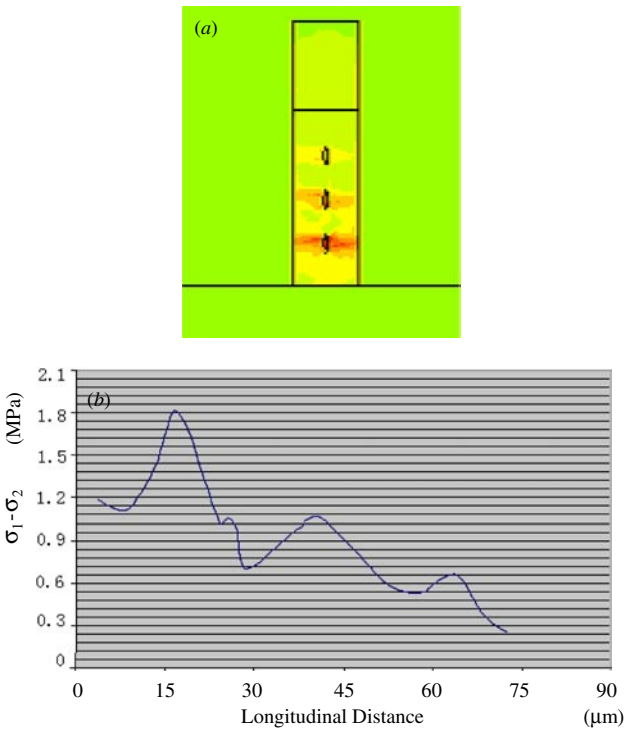

Figure 4. Stress distribution for SCR cantilevers. (*a*) differential stress distribution, (*b*) integrated differential stress along longitudinal axis.

of spring constant and resonance frequency for different geometries will help in designing the microchamber and controlling the flow rate to decrease the associated noise.

3.1.1. Stress concentration region: elliptical holes. Since the ratio ($\Delta R/R$) is proportional to the stress difference ($\Delta\sigma$), any geometrical enhancements to maximize the stress difference will result in increasing sensitivity of the biodetection process. For the finite element simulations, we have utilized elliptical holes located in the piezoresistor area to maximize the integrated stress difference. As shown in figure 3, three elliptical holes are located on the cantilever such that the distance between the holes are given by L_h, L_d is the distance between the first hole and the cantilever support, and W and L are the width and the length of the cantilever, respectively. For the simulation results shown in figure 4, $th = 0.1$ μm, $L = 120$ μm, $W = 30$ μm, $L_d = 15$ μm and $L_h = 12$ μm. In addition, $R_t = 2$ μm is the transverse axis length, $R_l = 8$ μm is length of the longitudinal axis and the hole axis hole ratio (R_l:R_t).

The value of the stress difference is concentrated around the holes, and is maximized around the first hole, which is closest to the supporting post (figure 4(*a*)). Three 'peaks' in

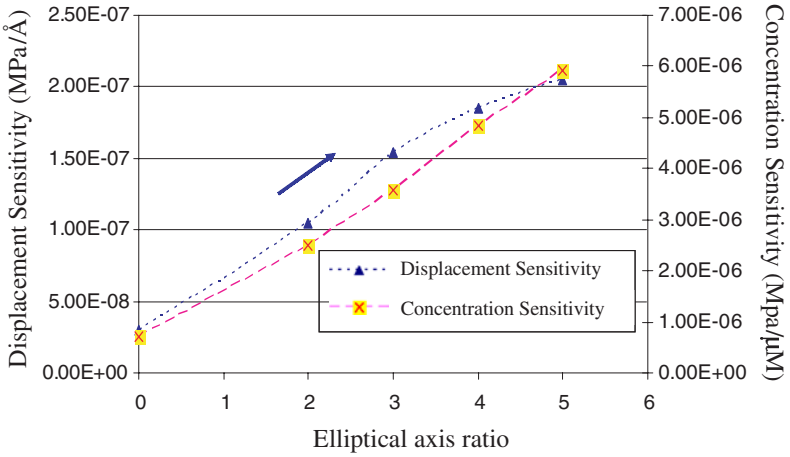

Figure 5. Displacement sensitivity, analyte concentration sensitivity for rectangular cantilever with different SCR axis ratio elliptical holes.

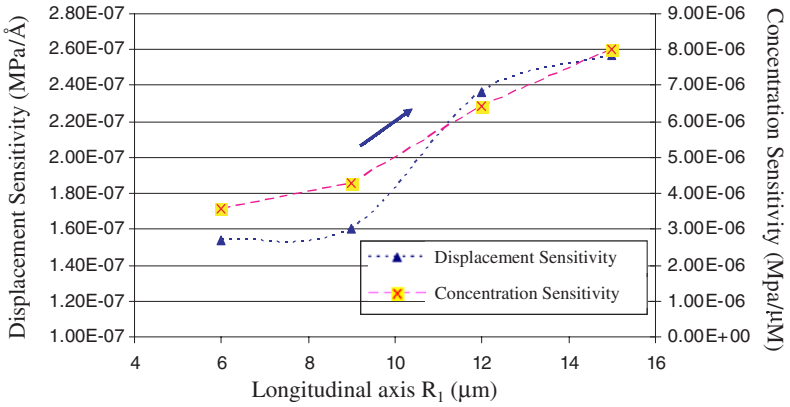

Figure 6. Parameters for SCR different hole scale size.

Table 3. Displacement sensitivity, analyte concentration sensitivity, spring constant and resonance frequency change for a rectangular cantilever with different SCR axis ratio elliptical holes.

Parameters	$L = 120\ \mu$m, $W = 30\ \mu$m (No SCR)	$R_l = 4\ \mu$m, $R_t = 2\ \mu$m, $th = 0.1\ \mu$m, $L_d = 15\ \mu$m, $L_h = 20\ \mu$m	$R_l = 6\ \mu$m, $R_t = 2\ \mu$m, $th = 0.1\ \mu$m, $L_d = 15\ \mu$m, $L_h = 20\ \mu$m	$R_l = 8\ \mu$m, $R_t = 2\ \mu$m, $th = 0.1\ \mu$m, $L_d = 15\ \mu$m, $L_h = 20\ \mu$m	$R_l = 10\ \mu$m, $R_t = 2\ \mu$m, $th = 0.1\ \mu$m, $L_d = 15\ \mu$m, $L_h = 20\ \mu$m
$\frac{\Delta R}{R} / (D\Pi)$ (MPa Å^{-1})	2.99×10^{-8}	1.05×10^{-7}	1.54×10^{-7}	1.85×10^{-7}	2.05×10^{-7}
$\frac{\Delta R}{R} / (C_0\Pi)$ (MPa μM^{-1})	7.16×10^{-7}	2.5×10^{-6}	3.58×10^{-6}	4.842×10^{-6}	5.92×10^{-6}
k (N m^{-1})	1.04×10^{-1}	9.24×10^{-2}	8.60×10^{-2}	7.64×10^{-2}	6.75×10^{-2}
F (kHz)	15.78	15.23	14.91	14.23	13.52

the integrated stress difference are observed near the holes, as shown in figure 4(*b*). Between the three peaks, we also observe two local minimum points or bottoms. Because the long axis of elliptical holes is along the longitudinal axis of cantilever, the effect of discontinuity causes the stress contours to change. A sharp increase in the differential stress is obtained on the cross section of the hole position. The effect of the stress concentration regions (SCRs) decreases sharply as we move away from the hole position (figure 4(*a*)).

Different axis ratios of elliptical holes have been utilized for the simulations, which resulted in different effects on the cantilever sensitivity, as shown in table 3 and figure 5, where C_0 is the initial surface analyte concentration, D is the displacement of the cantilever, k is the spring constant of the cantilever and F is the resonance frequency of the cantilever. Simulations have indicated that high axis ratio holes are always helpful to increase the stress difference, i.e. to increase the magnitude of the 'peaks' in the integrated stress difference, which results in increased signal sensitivity. Both the vertical displacement sensitivity and the analyte concentration sensitivity increase with the increase of axial ratio of the elliptical holes. Both the spring constant k and the resonance frequency F decrease with the increasing of the axis ratio.

In addition, changes in the size and thickness of the holes have effects on cantilever sensitivities, as shown in figures 6

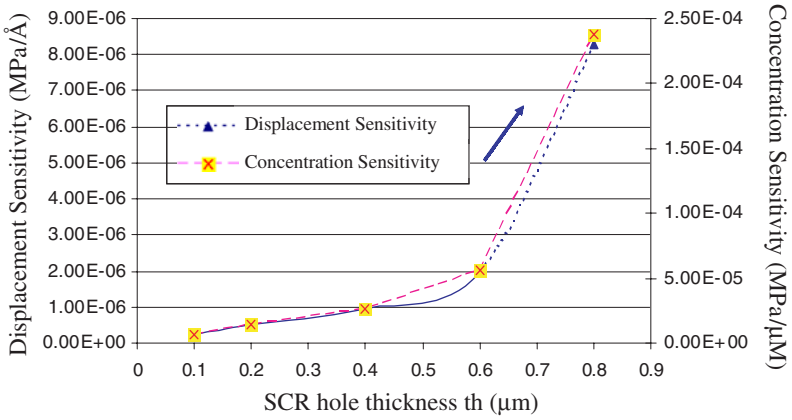

Figure 7. Parameters for SCR thickness.

Table 4. Parameters for SCR different hole scale size.

Parameters	$R_l = 6\ \mu m$, $R_t = 2\ \mu m$, $th = 0.1\ \mu m$, $L_d = 15\ \mu m$, $L_h = 20\ \mu m$	$R_l = 9\ \mu m$, $R_t = 3\ \mu m$, $th = 0.1\ \mu m$, $L_d = 15\ \mu m$, $L_h = 20\ \mu m$	$R_l = 12\ \mu m$, $R_t = 4\ \mu m$, $th = 0.1\ \mu m$, $L_d = 15\ \mu m$, $L_h = 20\ \mu m$	$R_l = 15\ \mu m$, $R_t = 5\ \mu m$, $th = 0.1\ \mu m$, $L_d = 15\ \mu m$, $L_h = 20\ \mu m$
$\frac{\Delta R}{R}\Big/(D\Pi)$(MPa Å^{-1})	1.54×10^{-7}	1.60×10^{-7}	2.36×10^{-7}	2.57×10^{-7}
$\frac{\Delta R}{R}\Big/(C_0\Pi)$(MPa μM^{-1})	3.58×10^{-6}	4.28×10^{-6}	6.42×10^{-6}	8.02×10^{-6}
k (N m^{-1})	8.60×10^{-2}	7.47×10^{-2}	7.35×10^{-2}	6.41×10^{-2}
F (kHz)	14.91	14.36	13.96	12.83

Table 5. Parameters for SCR thickness.

Parameters	$R_l = 12\ \mu m$ $R_t = 4\ \mu m$, $th = 0.1\ \mu m$, $L_d = 15\ \mu m$, $L_h = 20\ \mu m$	$R_l = 12\ \mu m$, $R_t = 4\ \mu m$, $th = 0.2\ \mu m$, $L_d = 15\ \mu m$, $L_h = 20\ \mu m$	$R_l = 12\ \mu m$, $R_t = 4\ \mu m$, $th = 0.4\ \mu m$, $L_d = 15\ \mu m$, $L_h = 20\ \mu m$	$R_l = 12\ \mu m$, $R_t = 4\ \mu m$, $th = 0.6\ \mu m$, $L_d = 15\ \mu m$, $L_h = 20\ \mu m$	$R_l = 12\ \mu m$, $R_t = 4\ \mu m$, $th = 0.8\ \mu m$, $L_d = 15\ \mu m$, $L_h = 20\ \mu m$
$\frac{\Delta R}{R}\Big/(D\Pi)$(MPa Å^{-1})	2.36×10^{-7}	5.34×10^{-7}	9.55×10^{-7}	1.98×10^{-6}	8.27×10^{-6}
$\frac{\Delta R}{R}\Big/(C_0\Pi)$(MPa μM^{-1})	6.42×10^{-6}	1.47×10^{-5}	2.68×10^{-5}	5.58×10^{-5}	2.38×10^{-4}
k (N m^{-1})	7.35×10^{-2}	7.29×10^{-2}	7.13×10^{-2}	7.09×10^{-2}	6.94×10^{-2}
F (kHz)	13.96	13.78	13.35	13.23	13.12

Table 6. Parameters for variable distance to support.

Parameters	$R_l = 8\ \mu m$, $R_t = 2\ \mu m$, $th = 0.1\ \mu m$, $L_h = 20\ \mu m$, $L_d = 25\ \mu m$	$R_l = 8\ \mu m$, $R_t = 2\ \mu m$, $th = 0.1\ \mu m$, $L_h = 20\ \mu m$, $L_d = 20\ \mu m$	$R_l = 8\ \mu m$, $R_t = 2\ \mu m$, $th = 0.1\ \mu m$, $L_h = 20\ \mu m$, $L_d = 15\ \mu m$	$R_l = 8\ \mu m$, $R_t = 2\ \mu m$, $th = 0.1\ \mu m$, $L_h = 20\ \mu m$, $L_d = 10\ \mu m$	$R_l = 8\ \mu m$, $R_t = 2\ \mu m$, $th = 0.1\ \mu m$, $L_h = 20\ \mu m$, $L_d = 5\ \mu m$
$\frac{\Delta R}{R}\Big/(D\Pi)$(MPa Å^{-1})	1.41×10^{-7}	1.56×10^{-7}	1.85×10^{-7}	2.13×10^{-7}	2.37×10^{-7}
$\frac{\Delta R}{R}\Big/(C_0\Pi)$(MPa μM^{-1})	2.67×10^{-6}	3.98×10^{-6}	4.84×10^{-6}	6.48×10^{-6}	7.82×10^{-5}
k (N m^{-1})	8.96×10^{-2}	8.42×10^{-2}	7.64×10^{-2}	6.57×10^{-2}	6.06×10^{-2}
F (kHz)	15.35	14.94	14.23	13.54	12.54

and 7. With an increase in the size or thickness of the holes, both the displacement and the analyte concentration sensitivities of the cantilever increase, and the spring constant and resonance frequency of the cantilever decrease. Overall, a large size hole, a large aspect ratio and a large thickness of the elliptical hole dimensions increase the sensitivity in spite of the slightly decreasing spring constant. Decreasing L_d will increase both the displacement and the analyte concentration sensitivities. In addition, the spring constant and resonance frequency of the cantilever will decrease (table 6). If we fix the location of the second hole in the cantilever and shorten the distance between the holes (L_h), both the displacement and the analyte concentration sensitivities will increase when L_h is decreased from 20 to 15 μm (figure 9).

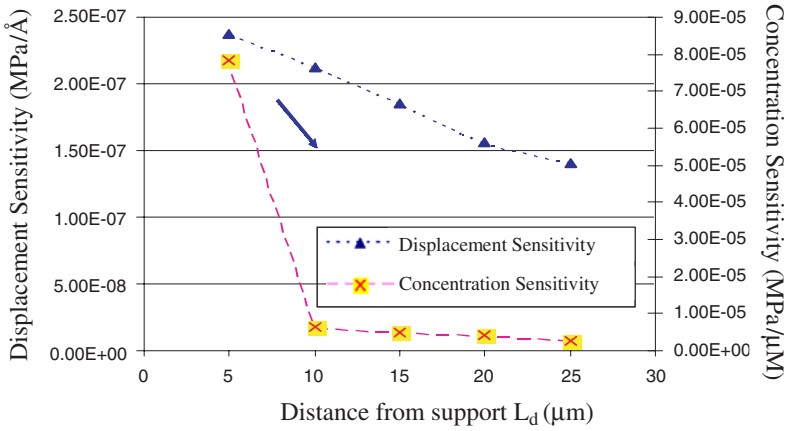

Figure 8. Parameters for variable distance to support.

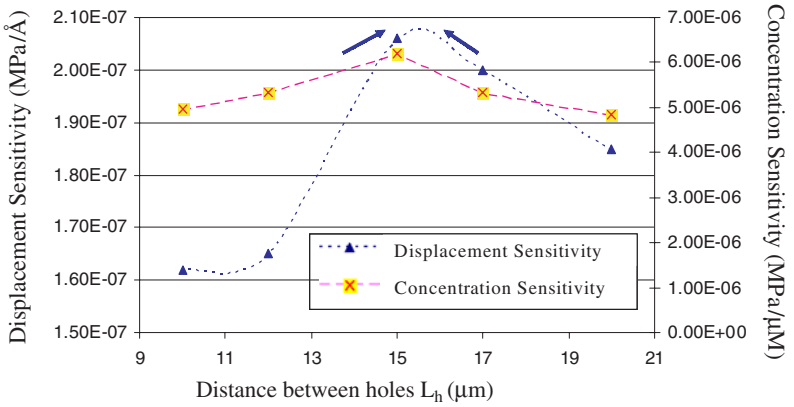

Figure 9. Parameters for variable distance between holes L_h.

Table 7. Parameters for variable distance between holes L_h.

Parameters	$R_l = 8\ \mu$m, $R_t = 2\ \mu$m, $th = 0.1\ \mu$m, $L_h = 20\ \mu$m	$R_l = 8\ \mu$m, $R_t = 2\ \mu$m, $th = 0.1\ \mu$m, $L_h = 17\ \mu$m	$R_l = 8\ \mu$m, $R_t = 2\ \mu$m, $th = 0.1\ \mu$m, $L_h = 15\ \mu$m	$R_l = 8\ \mu$m, $R_t = 2\ \mu$m, $th = 0.1\ \mu$m, $L_h = 12\ \mu$m	$R_l = 8\ \mu$m, $R_t = 2\ \mu$m, $th = 0.1\ \mu$m, $L_h = 10\ \mu$m
$\frac{\Delta R}{R}\Big/(D\Pi)$(MPa Å^{-1})	1.85×10^{-7}	2.00×10^{-7}	2.06×10^{-7}	1.65×10^{-7}	1.62×10^{-7}
$\frac{\Delta R}{R}\Big/(C_0\Pi)$(MPa μM^{-1})	4.84×10^{-6}	5.34×10^{-6}	6.20×10^{-6}	5.32×10^{-6}	4.96×10^{-6}
F (kHz)	14.23	13.46	13.55	13.50	13.38

Table 8. Parameters of variable width of cantilever.

Parameters	$L_v = 80\ \mu$m, $L_e = 40\ \mu$m, $W_e = 30\ \mu$m, $W_v = 30\ \mu$m	$L_v = 80\ \mu$m, $L_e = 40\ \mu$m, $W_e = 30\ \mu$m, $W_v = 25\ \mu$m	$L_v = 80\ \mu$m, $L_e = 40\ \mu$m, $W_e = 30\ \mu$m, $W_v = 20\ \mu$m	$L_v = 80\ \mu$m, $L_e = 40\ \mu$m, $W_e = 30\ \mu$m, $W_v = 15\ \mu$m	$L_v = 80\ \mu$m, $L_e = 40\ \mu$m, $W_e = 30\ \mu$m, $W_v = 10\ \mu$m	$L_v = 80\ \mu$m, $L_e = 40\ \mu$m, $W_e = 30\ \mu$m, $W_v = 5\ \mu$m
$\frac{\Delta R}{R}\Big/(D\Pi)$(MPa Å^{-1})	2.99×10^{-8}	3.71×10^{-7}	1.62×10^{-6}	2.28×10^{-7}	1.69×10^{-7}	1.04×10^{-7}
$\frac{\Delta R}{R}\Big/(C_0\Pi)$(MPa μM^{-1})	7.14×10^{-7}	1.59×10^{-5}	3.06×10^{-5}	1.66×10^{-5}	7.60×10^{-6}	6.32×10^{-6}
F (kHz)	15.78	14.26	13.34	12.45	10.16	8.089

If L_h is decreased further, both sensitivities will also start to decrease. We conclude that the optimum distance between the holes can be taken to be twice the long axis length.

3.1.2. Variable width of cross section. Simulations have indicated that variable width of the cantilever geometry can be used to increase the sensitivity. W_v is the width of the cantilever near the support, W_e is the width of the

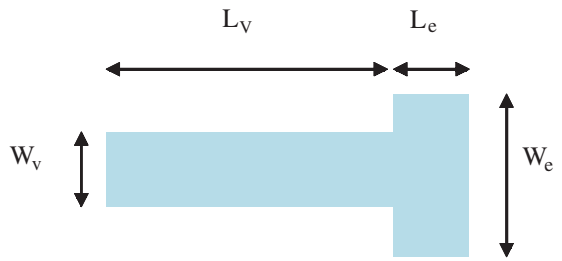

Figure 10. Geometry parameters for variable cross section.

cantilever at the end, L_v is the length of cantilever close to the support and L_e is the length of cantilever at the end (figure 10). The displacement and the analyte concentration sensitivities increase when W_v decreases from 30 to 20 μm (figure 11). This is because the differential stress reaches the maximum around $W_v = 20$ μm for the increasing extent of the SCR. When W_v decreases further, the decrease in the cantilever spring constant will dominate, and hence both the displacement and the analyte concentration sensitivities will decrease. Since the ratio L_v:L_e = 3:2, it is reasonable to find that the maximum sensitivity is obtained when W_e:W_v = 3:2.

3.2. Design principles

From the previous analysis, we can conclude the following.

(1) The differential stress ($\sigma_1 - \sigma_2$) is concentrated in the area near the support post.
(2) SCR (holes) can increase the magnitude of the differential stress ($\sigma_1 - \sigma_2$). In the case of elliptical holes, a large axis ratio, large hole dimensions and deep hole thickness can increase both the displacement and analyte concentration sensitivities even though the cantilever spring constant decreases.
(3) For integrated differential stress ($\sigma_1 - \sigma_2$), the peaks are obtained in positions around the holes.
(4) The optimal distance between holes is taken to be twice the longitudinal axis of elliptical holes.
(5) Moving holes closer to the support increases both the displacement and the analyte concentration sensitivities.

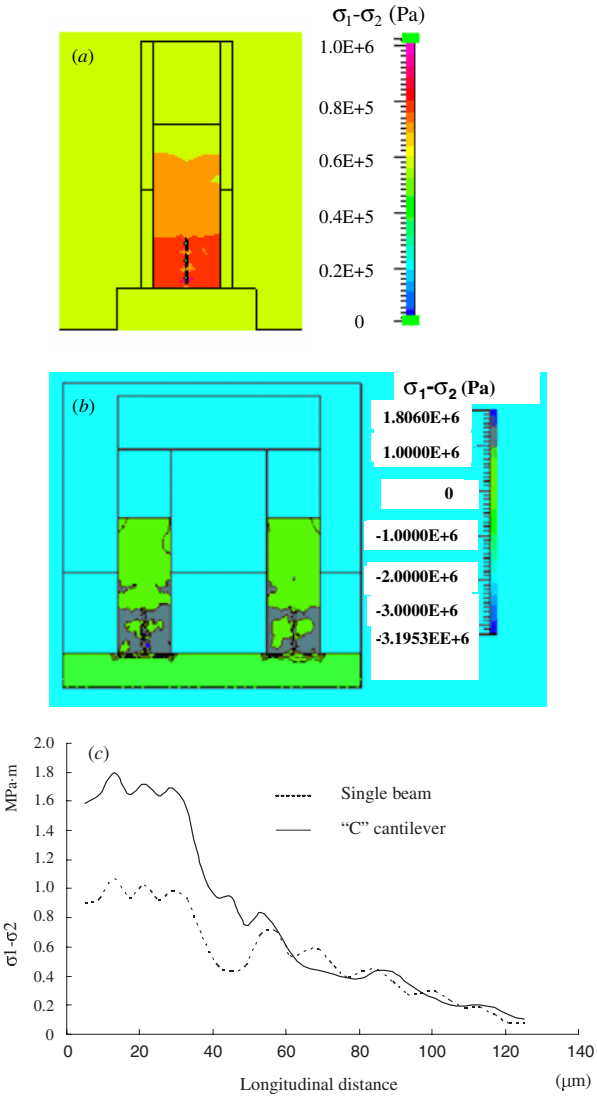

Figure 12. (*a*) Differential stress distribution of normal cantilever, (*b*) differential stress distribution of 'C' modified cantilever and (*c*) integrated differential stress along longitudinal axis.

(6) Decreasing the cross section close to the support will increase the displacement and analyte concentration

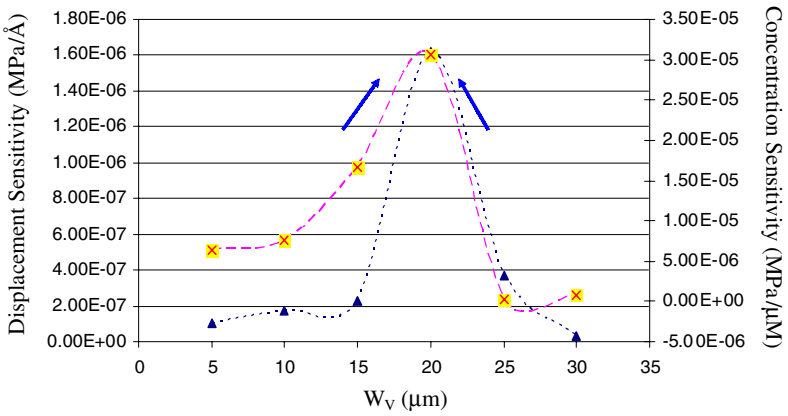

Figure 11. Parameters of variable width of cantilever.

Table 9. Parameters for 'C' cantilevers.

Parameters	$R_l = 6\ \mu$m, $R_t = 2\ \mu$m, $th = 1\ \mu$m	$R_l = 9\ \mu$m, $R_t = 3\ \mu$m, $th = 1\ \mu$m	$R_l = 12\ \mu$m, $R_t = 4\ \mu$m, $th = 1\ \mu$m
$\frac{\Delta R}{R}\Big/(D\Pi)$ (MPa Å^{-1})	2.35×10^{-7}	3.77×10^{-7}	8.45×10^{-7}
$\frac{\Delta R}{R}\Big/(C_0\Pi)$ (MPa μM^{-1})	1.53×10^{-5}	5.82×10^{-5}	9.46×10^{-5}

Table 10. Geometrical parameters for the optimized SCR modified 'C' cantilever.

Parameters	Nomenclature
Length of cantilever, L	$L = 120\ \mu$m
Width of cantilever, W	$W = 30\ \mu$m
Contacting beam	$30 \times 120\ \mu$m^2
Thickness of elliptical holes, t	$th = 1\ \mu$m
Transverse axis length of elliptical holes	$R_t = 4\ \mu$m
Longitudinal axis length of elliptical holes	$R_l = 12\ \mu$m
Distance between elliptical holes	$L_h = 15\ \mu$m
Distance between the first hole and the support	$L_d = 1\ \mu$m

sensitivities. The sensitivities first reach the maximum and then decrease. An optimum ratio is L_v:$L_e = W_e$:W_v.

3.3. Optimized stress concentration region modified 'C' cantilever based on the design principle

Based on the design principle discussed previously, the optimized SCR modified 'C' cantilever is designed to increase the overall detection sensitivity. For the simulations whose results are presented below, the holes are moved towards the support, the distance between the holes is shortened, and large size, large aspect ratio and large depth for the holes are assumed. In figure 12(*c*), the overlap of the three 'peaks' and hence a comparatively stable flat roof area can be found near the support area. This is where the piezoresistive layer should be located to collect large signals. The normal single beam cantilever is also compared with the 'C' cantilever with the same optimized geometry factors and the same initial concentration. The 'C' cantilever has a higher differential stress than the single beam cantilever because of the increasing binding area on the connecting beam far away from the support, which significantly increases the differential stress on the cantilever (figure 12(*c*)). The principles outlined previously for the optimal design of rectangular cantilevers are also useful for the design of 'C'-shaped cantilevers (table 9).

4. Conclusion

We have developed a finite element computational model for simulating the chemo-mechanical binding of analytes to specific binding molecules on functionalized surfaces. The analyte concentration is uniformly distributed over the reaction surface when the analyte concentration reaches a saturated level. This means that the stable chemo-mechanical binding stress gives rise to a uniform distribution for surface stress which can be utilized for bio-sensing using a cantilevered detection system. Displacement and uniformly distributed force sensitivity analysis have been carried out to investigate the effects of geometrical factors on the piezoresistive cantilever. Optimization of geometry factors can increase the device sensitivity to the binding and hybridization of biomolecules. Design principles are established according to the geometry analysis. Finally, the optimum SCR modified 'C' piezocantilever system for biosensing is designed and the optimal parameters are set for the high sensitivity (table 10).

References

[1] Raiteri R, Nelles G, Butt H-J, Knoll W and Skladal P 1999 Sensing of biological substances based on the bending of microfabricated cantilevers *Sensors Actuators* B **61** 213–7

[2] Jensenius H, Thaysen J, Rasmussen A, Veje H L, Hansen O and Boisen A 2000 A mircrocantilever-based alcohol vapor sensor-application and response model *Appl. Phys. Lett.* **76** 2615–7

[3] Hansen A, Mortensen M W, Anderson J, Ulstrop J, Kuhle A, Garnaes J and Boisen A 2001 Stress formation during self-assembly of alkanethiols on differently pre-treated gold surfaces *Probe Microsc.* **2** 139–49

[4] Bauer P, Hecht B and Rossel C 1995 Piezoresistive cantilevers as optical sensors for scanning near-field microscopy *Ultramicroscopy* **61** 127–30

[5] Brugger J, Buser R A and de Rooij N F 1992 Micromachined atomic force microprobe with integrated capacitive read-out *J. Micromech. Microeng.* **2** 218–20

[6] Dragoman D and Dragoman M 2001 Terahertz field characterization using Fabry-Perot-like cantilevers *Appl. Phys. Lett.* **79** 581–3

[7] Grabiec P, Gotszalk T, Radojewski J, Edinger K, Abedinov N and Rangelow I W 2002 SNOM/AFM microprobe integrated with piezoresistive cantilever beam for multifunctional surface analysis *Microelectron. Eng.* **61–62** 981–6

[8] Kassegne S, Madou J M, Whitten R, Zoval J, Mather E, Sarkar K, Hodko D and Maity S 2002 Design issues in SOI-based high-sensitivity piezoresistive cantilever devices *Proc. SPIE Conf. on Smart Structures and Materials (San Diego, CA, 17–21 March)*

[9] Harley J A and Kenny T W 1999 High-Sensitivity Cantilevers Under 1000A Thick *Appl. Phys. Lett.* **75** 289–91

[10] Lavrik N V, Tipple C A, Sepaniak M J and Datskos D 2001 Gold nanostructure for transduction of biomolecular interactions into micrometer scale movements *Biomed. Microdevices* **3** 35–44

[11] Chang K-C and Hammer D A 1999 The forward rate of binding of surface-tethered reactants: effect of relative motion between two surfaces *Biophys. J.* **76** 1280–92

[12] Swift D G, Posner R G and Hammer D A 1998 Kinetics of adhesion of IgE sensitized rat basophilic leukemia cells to surface-immobilized antigen in Couette flow *Biophys. J.* **75** 2597–611

[13] Ramakrishnan A and Sadana A 2000 A predictive approach using fractal analysis for analyte-receptor binding and dissociation kinetics for surface plasmon resonance biosensor applications *J. Interface Colloid Sci.* **229** 628–40

[14] Pritchard W F, Davis P F, Derafshi Z, Polacek D C, Tsoa R, Dull R O, Jones S A and Giddens D P 1995 Effects of wall shear stress and fluid recirculation on the localization of circulating monocytes in a three-dimensional flow model *J. Biomech.* **28** 1459–69